Supplemental material

Ripoll et al., https://doi.org/10.1083/jcb.201709055

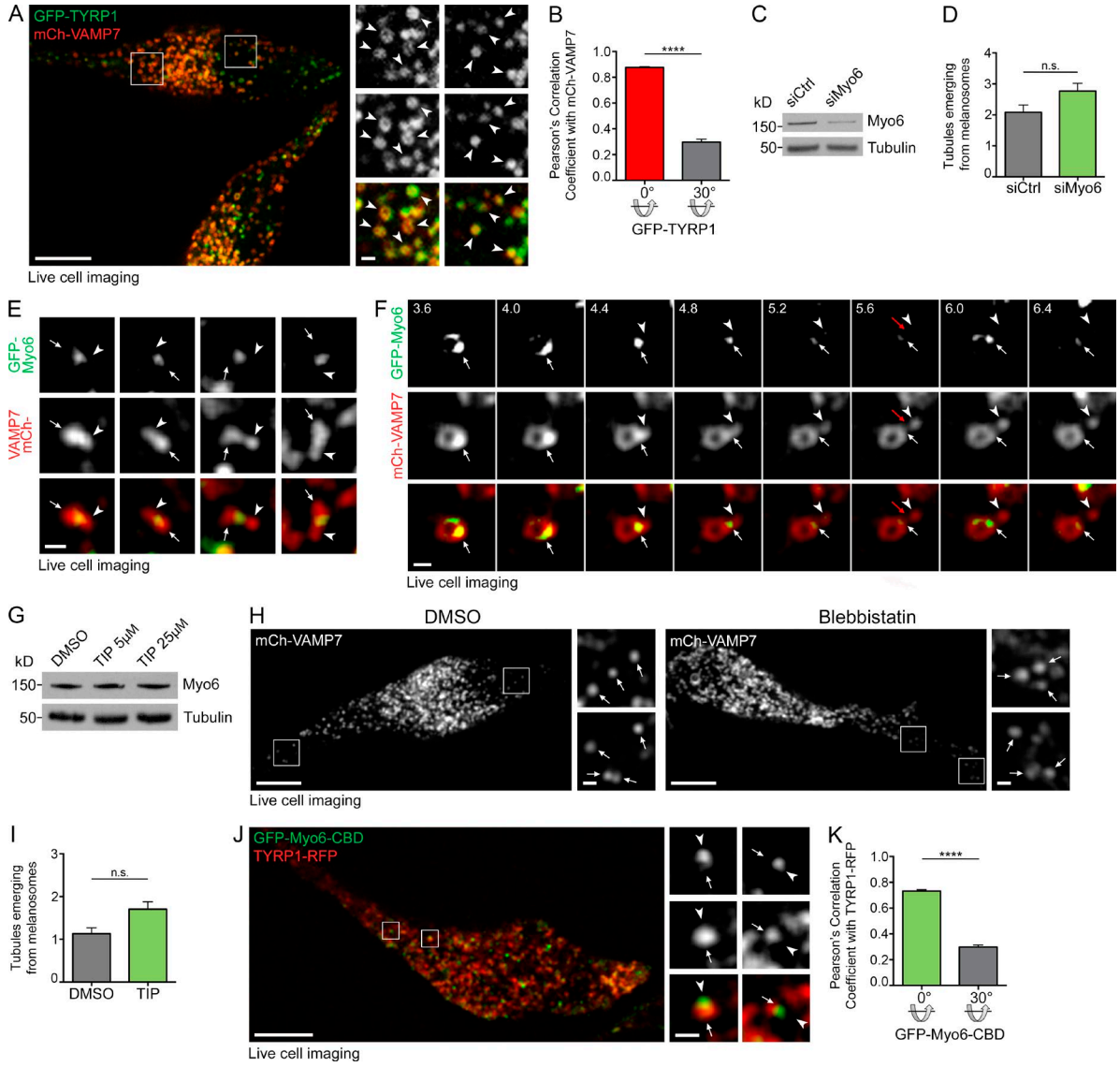

Figure S1. **Myo6 expression and activity are required for the release of melanosomal tubules. (A and B)** Live imaging frame of GFP-TYRP1 and mCh-VAMP7 expressing MNT-1 cells (A) and associated Pearson's correlation coefficient (B, *n* = 43 cells). Control values were obtained by 30° rotation of the GFP channel of the same images. Arrowheads in 2.5× magnified box areas show colocalization. **(C)** Western blot analysis of control- or Myo6-depleted lysates probed for the respective antibodies; tubulin serves as loading control. **(D)** Relative number of emerging mCh-VAMP7$^+$ melanosomal tubules from 256-µm^2 area of cells treated as in A during 40-s live acquisition (siCtrl, *n* = 4 independent experiments; siMyo6, *n* = 3 independent experiments). **(E)** Frames from a live imaging sequence of GFP-Myo6– and mCh-VAMP7–expressing MNT-1 cells. GFP-Myo6 localizes to the intersection between the melanosome cores (arrows) and the associated tubules (arrowheads). **(F)** Consecutive time-lapse images show a mCh-VAMP7$^+$ tubule (arrowheads) emerging and detaching (red arrow) from a GFP-Myo6$^+$ melanosome subdomain (arrows) over time (s). **(G)** Western blot analysis of MNT-1 cell lysates treated for 30 min with DMSO, 5 µM TIP, or 25 µM TIP and probed with Myo6 or tubulin antibodies. **(H)** Live imaging frame of mCh-VAMP7–expressing MNT-1 cells treated for 60 min with DMSO or 50 µM blebbistatin. Magnified views are 3× of boxed area. **(I)** Relative number of emerging mCh-VAMP7$^+$ melanosomal tubules from a 256-µm^2 area of DMSO- or 5 µM TIP–treated MNT-1 cells during 40-s live acquisition (DMSO, *n* = 3 independent experiments; TIP, *n* = 3 independent experiments). **(J)** Live imaging frame of GFP-Myo6-CBD and TYRP1-RFP expressing MNT-1 cells. Magnified boxed areas (4×) show GFP-Myo6-CBD$^+$ spots (arrowheads) associated with TYRP1-RFP$^+$ melanosomes (arrows). **(K)** Pearson's correlation coefficient of cells (*n* = 45 cells) as in H. Control values were obtained by 30° rotation of the GFP layer of the same images. Molecular mass in kilodaltons. Data are presented as the mean ± SEM. Bars: (A, H, and J) 10 µm; (E and F and magnifications in A, H, and J) 1 µm. ****, P < 0.0001; n.s., not significant (unpaired *t* test).

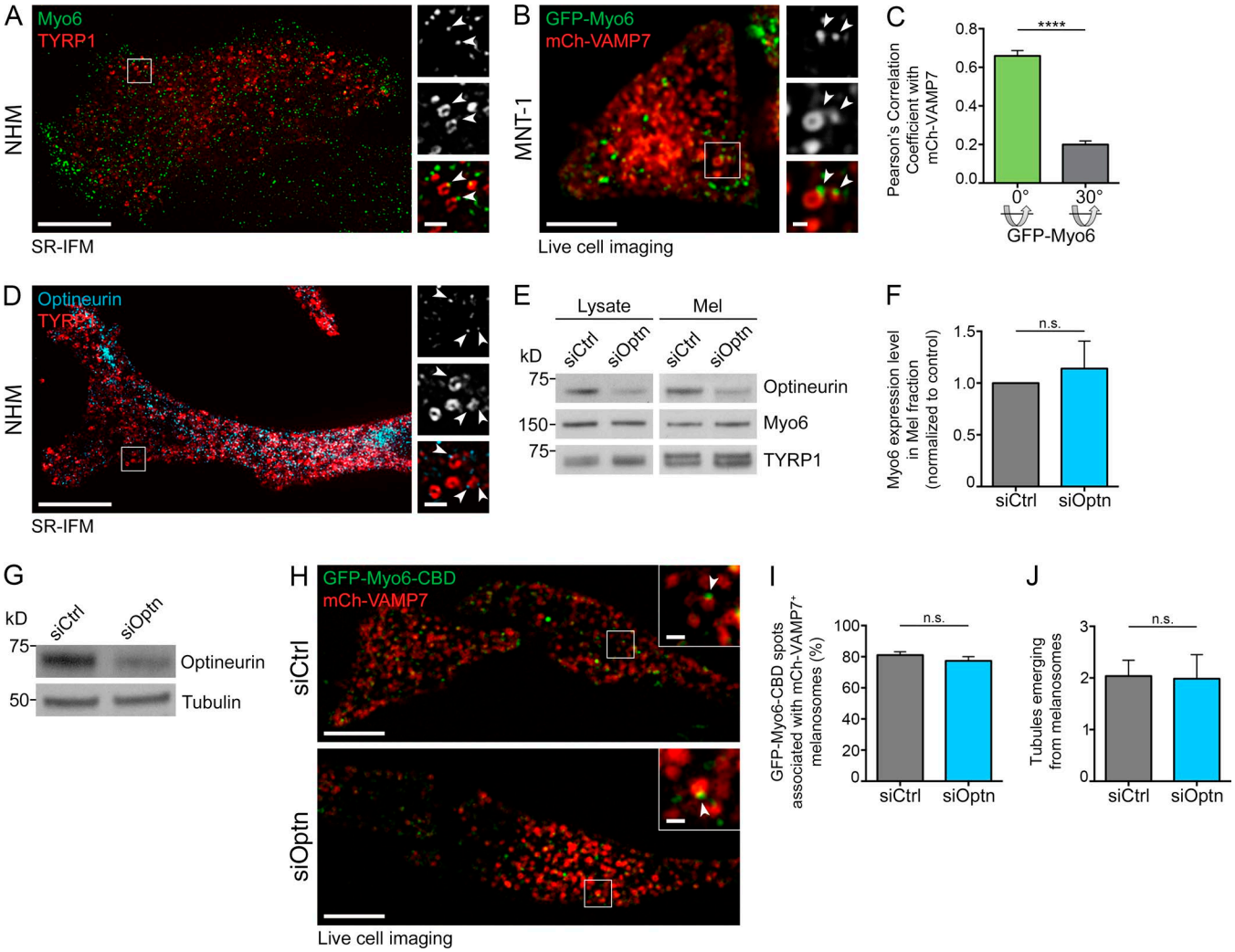

Figure S2. **Optineurin does not recruit Myo6 to melanosomes. (A)** SR-IFM on NHM costained for endogenous Myo6 and TYRP1. Myo6 (arrowheads; 3× of boxed area) localizes to TYRP1⁺ melanosomal subdomain. **(B and C)** Live imaging frame of GFP-Myo6-CBD and mCh-VAMP7 coexpressing MNT-1 cells (B) and corresponding Pearson's correlation coefficient (C; *n* = 27 cells). GFP-Myo6 (B, arrowheads; 2× of boxed regions) localizes to mCh-VAMP7⁺ melanosomal subdomain. **(D)** SR-IFM on NHM costained for endogenous optineurin and TYRP1. Optineurin (arrowheads; 3× of boxed area) localizes to TYRP1⁺ melanosomal subdomain. **(E)** Western blot analysis of whole-cell lysates and melanosome-enriched fractions (Mel) isolated from control or optineurin siRNA-treated MNT-1 cells and probed for the respective antibodies. **(F)** Quantification of Myo6 protein expression level on Mel fraction and normalized to control (*n* = 3 independent experiments). **(G)** Western blot analysis of control or optineurin-depleted MNT-1 cell lysates probed for the respective antibodies. **(H)** Live imaging frames of MNT-1 cells treated with control or optineurin siRNAs and transfected with GFP-Myo6-CBD and mCh-VAMP7. Magnified areas (3×) show GFP-Myo6-CBD⁺ spots (arrowheads) associated with mCh-VAMP7⁺ melanosomes. **(I)** Percentage of GFP-Myo6-CBD⁺ spots associated with mCh-VAMP7⁺ melanosomes in cells as in H (siCtrl, *n* = 24 cells; siOptn, *n* = 21 cells). **(J)** Relative number of mCh-VAMP7⁺ tubules emerging from melanosomes of control or optineurin-depleted cells from 256-µm² area during 40-s live acquisition (siCtrl, *n* = 4 independent experiments; siOptn, *n* = 3 independent experiments). Molecular mass in kilodaltons. Data are presented as the mean ± SEM. Bars: (A, B, D, and H) 10 µm; (A, B, D, and H, magnifications) 1 µm. ****, P < 0.0001, n.s., not significant (unpaired *t* test).

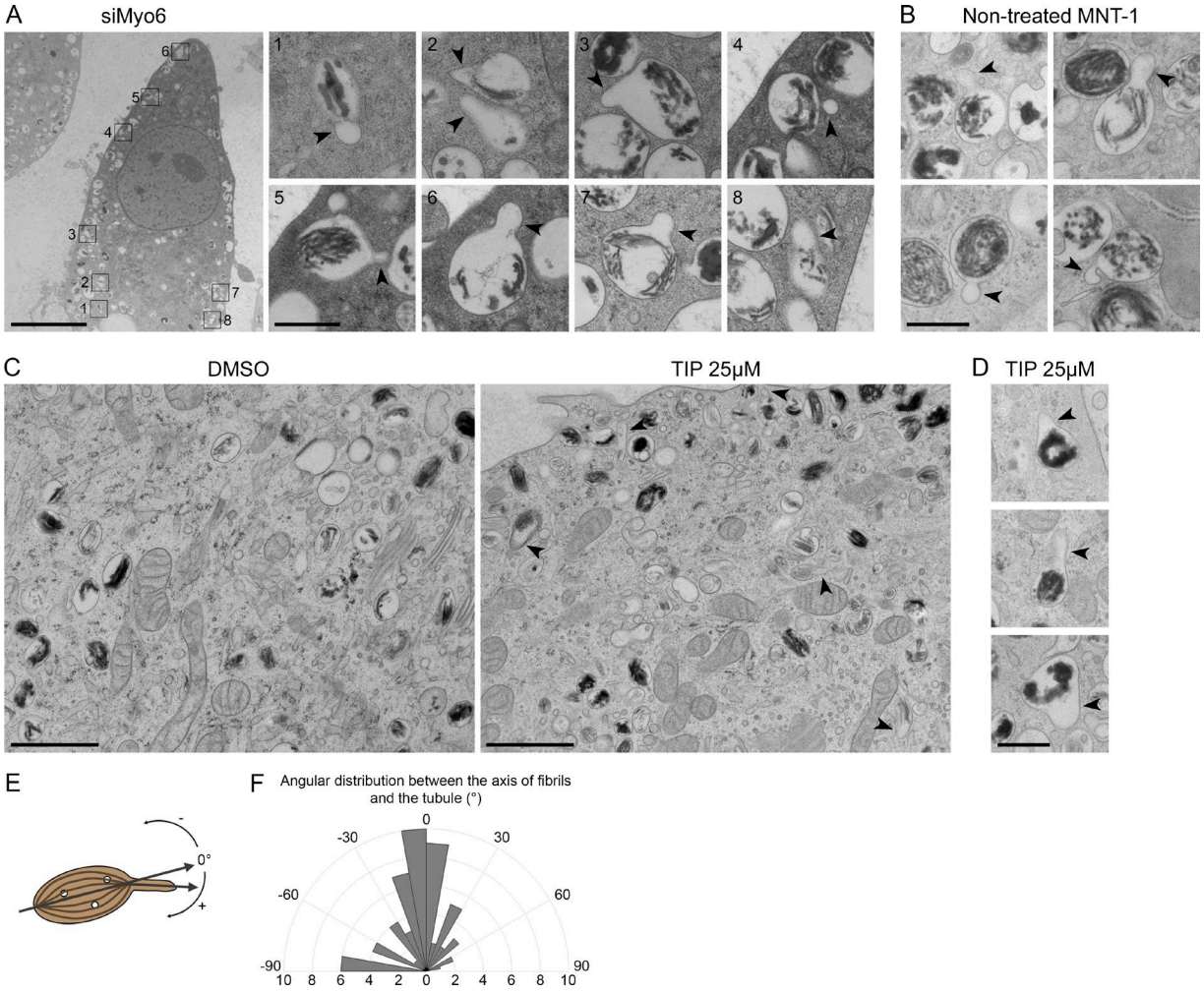

Figure S3. **Fission of melanosomal tubules requires Myo6 expression and activity. (A and B)** Electron micrographs from MNT-1 cells treated with Myo6 siRNA (A, overview and gallery) or not treated (B). **(C and D)** Electron micrographs from MNT-1 cells treated for 1 h with DMSO or 25 µM TIP. Arrowheads indicate tubules connected to melanosomes (A–D). **(E and F)** Diagram (E) and quantification (F) of the angle distribution between the long axis of the fibrils and the tubule on n melanosomes (n = 60). Quantification is based on tubules from siCtrl and siMyo6-treated cells. Bars: (A, overview) 5 µm; (C) 1 µm; (A, magnified gallery; and B and D) 500 nm.

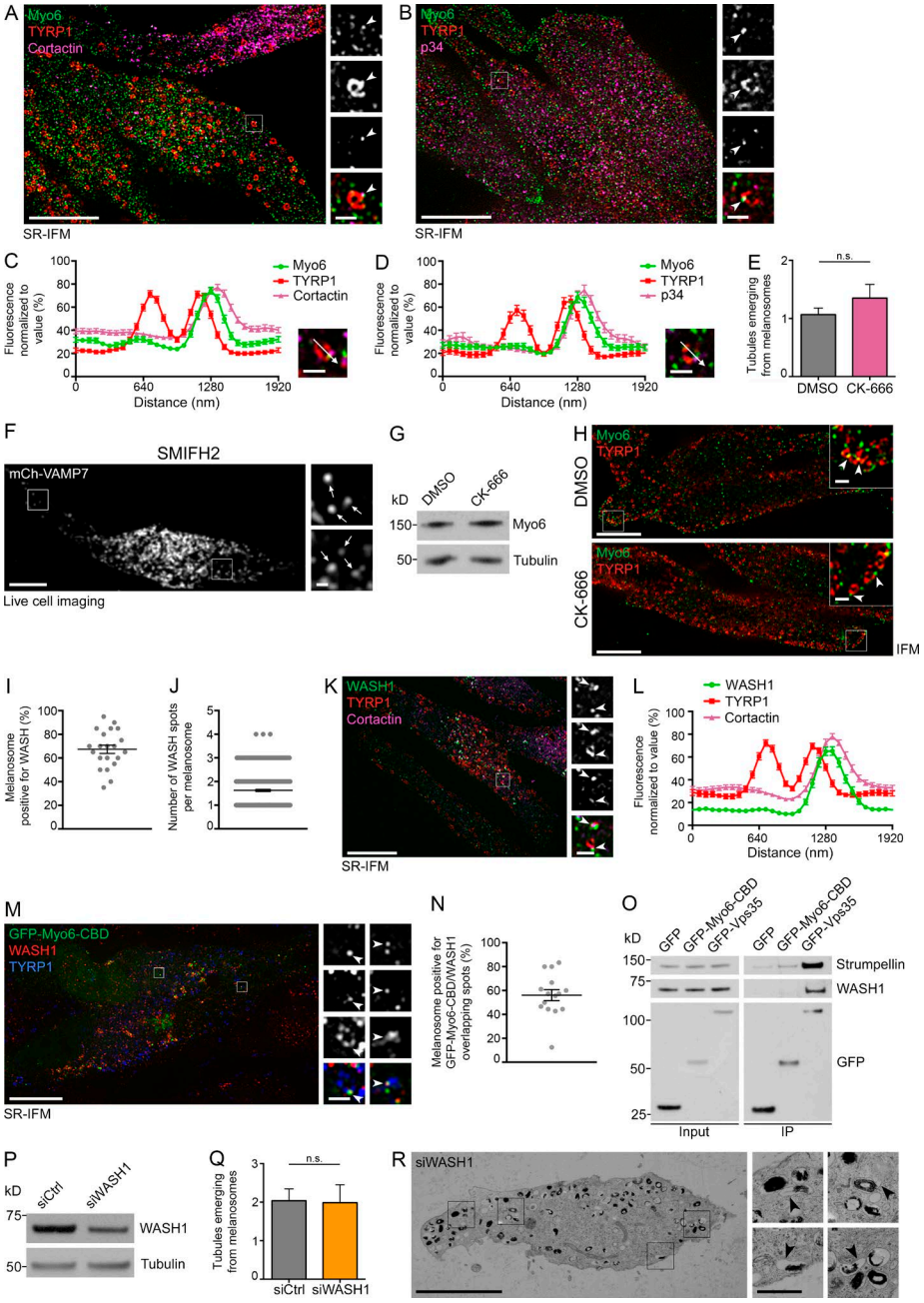

Figure S4. **Arp2/3, WASH, and branched actin distribute with Myo6 and control the fission of melanosomal tubules. (A and B)** SR-IFM on MNT-1 cells labeled for endogenous Myo6, TYRP1, and cortactin (A) or p34 (B); Myo6 colocalizes with cortactin or p34 (arrowheads; 3× of boxed area) on TYRP1$^+$ melanosomes. **(C and D)** Linear pixel values across *n* TYRP1$^+$ melanosomes show cortactin (C) or p34 (D) fluorescence enrichment together with Myo6 at melanosomal subdomain (cortactin, $n = 69$; p34, $n = 41$). **(E)** Relative number of mCh-VAMP7$^+$ tubules emerging from melanosomes in cells (256-µm^2 area) treated with DMSO or 50 µM CK-666 during 40-s live acquisition ($n = 3$ independent experiments). **(F)** Live imaging frame of MNT-1 cells treated with 50 µM SMIFH2. Magnified views are 3× of boxed area. **(G and H)** MNT-1 cells treated with DMSO or 50 µM CK-666 were analyzed by Western blot (G) or IFM (H) and stained for Myo6 (H; arrowheads, 3× of boxed area) with tubulin or TYRP1, respectively. **(I and J)** Percentage of WASH1/TYRP1$^+$ melanosomes (I; $n = 21$ cells), and relative number of WASH1$^+$ fluorescent spots per melanosome (J; $n = 420$ melanosomes). **(K)** SR-IFM on MNT-1 cells labeled for endogenous WASH1, TYRP1, and cortactin. WASH1 and cortactin codistribute with melanosome (arrowheads; 3× of boxed area). **(L)** Linear pixel values across TYRP1$^+$ melanosomes show WASH1-associated fluorescence enriched at a melanosomal subdomain ($n = 100$ melanosomes). **(M)** SR-IFM of GFP-Myo6-CBD–expressing MNT-1 cells stained for endogenous WASH1 and TYRP1. Magnified areas (4×) show WASH1 and GFP-Myo6-CBD colocalization to TYRP1$^+$ melanosomes. **(N)** Percentage of melanosomes with GFP-Myo6-CBD and WASH1 overlapping spots ($n = 15$ cells). **(O)** Western blot analysis of lysates (input) and GFP IP of GFP-, GFP-Myo6-CBD–, or GFP-Vps35–expressing MNT-1 cells probed for the respective antibodies. **(P)** Western blot of lysates of MNT-1 cells treated with control or WASH1 siRNAs and probed for WASH1 and tubulin as a loading control. **(Q)** Relative number of mCh-VAMP7$^+$ tubules emerging from melanosomes in control- or WASH-depleted cells (256-µm^2 area) during 40-s live acquisition (siCtrl, $n = 4$ independent experiments; siWASH1, $n = 3$ independent experiments). **(R)** HPF and conventional EM on WASH1-depleted MNT-1 cells. Tubules connected to melanosomes are highlighted (arrowheads). Molecular mass is in kilodaltons. Data are presented as the mean ± SEM. Bars: (A, B, F, H, K, and M) 10 µm; (R) 5 µm; (A–D, F, H, K, M, and R, magnifications) 1 µm. n.s., not significant (unpaired *t* test).

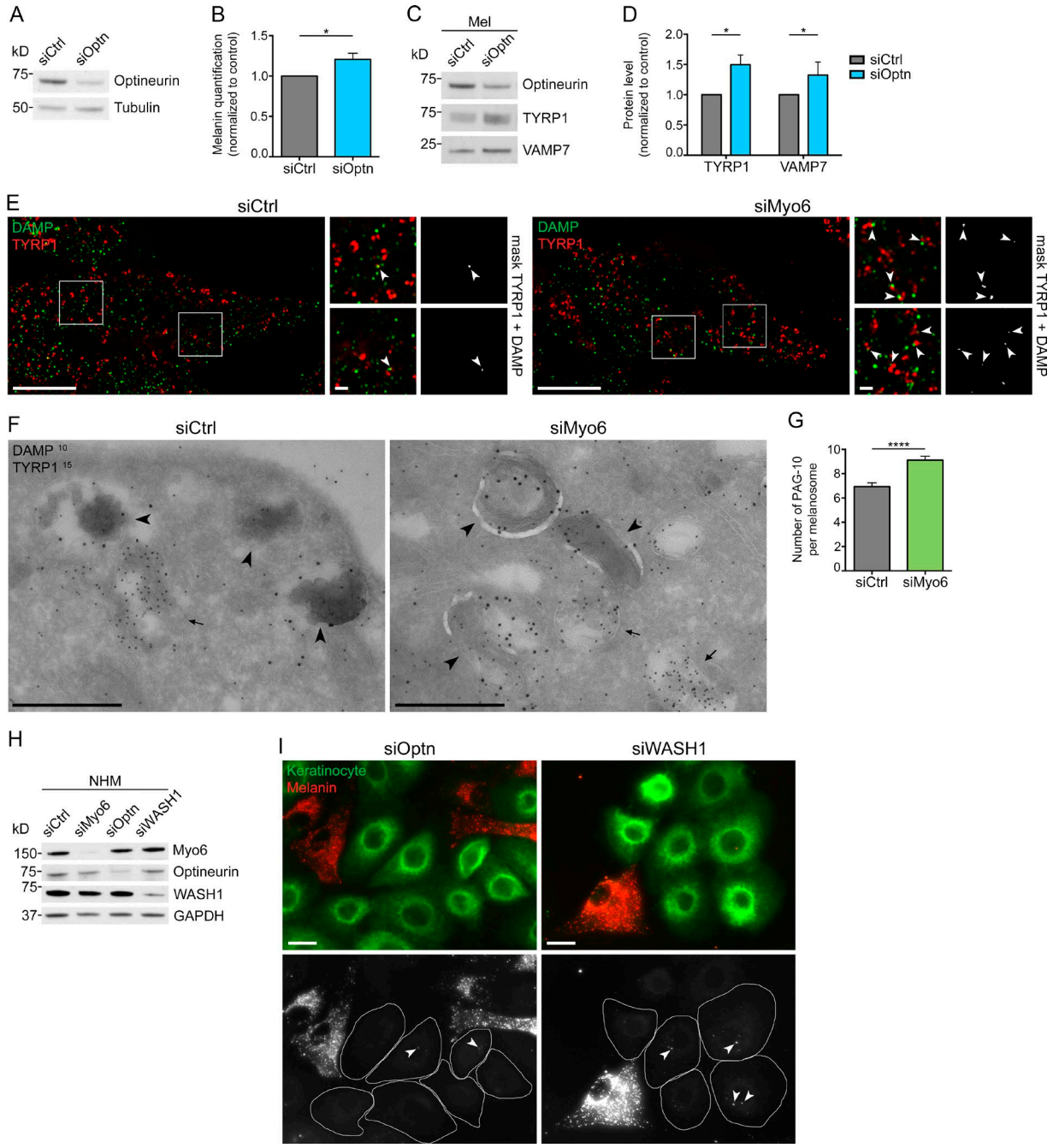

Figure S5. **Myo6 expression impacts the intraluminal pH of melanosomes. (A)** Western blot analysis of lysates of MNT-1 cells treated with control or optineurin siRNAs and probed for respective antibodies. **(B)** Intracellular melanin estimation of control- or optineurin-depleted MNT-1 cells (n = 5 independent experiments; normalized to control). **(C)** Western blot of melanosome subcellular fractions (Mel) from control- or optineurin-depleted MNT-1 cells probed with respective antibodies. **(D)** Quantification of TYRP1 and VAMP7 protein expression levels on Mel fractions in C and normalized to control (n = 3 independent experiments). **(E and F)** control- or Myo6-depleted MNT-1 cells incubated for 30 min with 30 µM DAMP were processed and analyzed by IFM (E) or IEM (F) using antibodies to dinitrophenol (DNP; to label DAMP) and TYRP1. **(E)** DAMP (green) and TYRP1 (red) puncta are partially overlapping (arrowheads; 2× of boxed area) as shown on the colocalization masks. **(F)** DAMP (PAG 10 nm) staining localizes to the lumen of TYRP1$^+$ pigmented melanosome (PAG 15 nm; arrowheads), and to immature unpigmented melanosomes (arrows; known as acidic compartments that accumulate DAMP staining; Anderson et al., 1984; Raposo et al., 2001). **(G)** Quantification of the number of DNP-associated gold particles per n pigmented melanosome (F, arrowheads) on ultrathin cryosections (siCtrl, n = 355; siMyo6, n = 535). **(H)** Western blot analysis of lysates of NHMs treated with control, Myo6, optineurin, or WASH1 siRNAs and probed with respective antibodies. **(I)** IFM of NHMs treated with control, optineurin, or WASH1 siRNAs co-cultured with NHKs and stained for HMB45 (red) or EGFR (green) identifying melanin and NHMs or NHKs, respectively. HMB45 staining within NHKs (arrowheads) correspond to the transferred melanin. Molecular mass is in kilodaltons. Data are presented as the mean ± SEM. Bars: (E and I) 10 µm; (E, magnifications) 1 µm; (F) 500 nm. ****, $P < 0.0001$; *, $P < 0.05$ (unpaired t test).

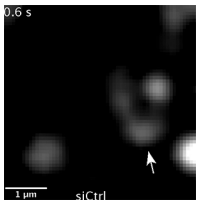

Video 1. **VAMP7 tubule emerges and detaches from the melanosome.** Spinning-disc confocal microscopy on MNT-1 cells expressing mCh-VAMP7 that localizes to melanosomes. A VAMP7⁺ tubular structure (arrowhead) emanating from the core of a melanosome (arrow) detaches and disappears rapidly from the field of view (see also Fig. 1 B). Acquisition parameters: 200 ms exposure, one z-stack (0.2 µm). Video is shown at four frames per second. Bar, 1 µm.

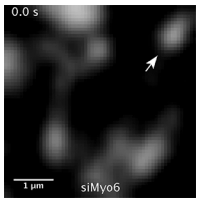

Video 2. **Myo6 depletion impairs the release of VAMP7 tubules from melanosomes.** Spinning-disc confocal microscopy on Myo6-depleted MNT-1 cells expressing mCh-VAMP7 shows a VAMP7⁺ tubular structure (arrowhead) associated with the melanosome (arrow). The tubule stays associated with the melanosome core and fails to detach over time acquisition (see also Fig. 1 H). Acquisition parameters: 200 ms exposure, one z-stack (0.2 µm). Video is shown at seven frames per second. Bar, 1 µm.

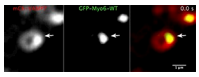

Video 3. **GFP-Myo6 localizes to a melanosomal subdomain from which a mCh-VAMP7 tubule emerges and is released.** Spinning-disc confocal microscopy of MNT-1 cells expressing GFP-Myo6 and mCh-VAMP7. A VAMP7⁺ tubular structure (arrowhead) emanating from a GFP-Myo6⁺ melanosomal subdomain (arrow) detaches and disappears rapidly from the field of view (see also Fig. S1 F). Acquisition parameters: 200 ms exposure, one z-stack (0.2 µm). Video is shown at seven frames per second. Bar, 1 µm.

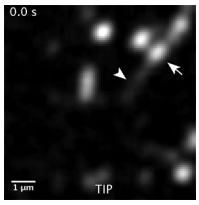

Video 4. **Inhibiting the Myo6 motor activity prevents the release of VAMP7 tubules from melanosomes.** Spinning-disc confocal microscopy on MNT-1 cells expressing mCh-VAMP7 and incubated for 30 min with 5 µM TIP shows two melanosomes (arrows) associated each with a VAMP7⁺ tubular structure (arrowheads). The tubules remain stably associated with the melanosome core and fail to detach over time acquisition (see also Fig. 1 I). Acquisition parameters: 200 ms exposure, one z-stack (0.2 µm). Video is shown at seven frames per second. Bar, 1 µm.

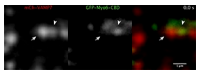

Video 5. **GFP-Myo6-CBD localizes to melanosomes associated with mCh-VAMP7 tubules.** Spinning-disc confocal microscopy on MNT-1 cells expressing mCh-VAMP7 (red, left panel) and GFP-Myo6-CBD (green, middle panel) shows the core of a VAMP7⁺ melanosome (arrow) associated with a tubular structure (arrowhead) to which GFP-Myo6-CBD is localized (see also Fig. 1 L). At least two GFP-Myo6-CBD⁺ fluorescent spots are associated with the melanosome, among which one remains localized to the tubule that fails to detach over time. The merged channel was shown (right). Acquisition parameters: 200 ms exposure, one z-stack (0.2 µm). Video is shown at seven frames per second. Bar, 1 µm.

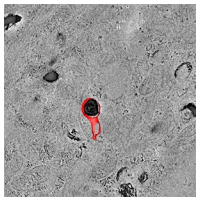

Video 6. **3D model at the ultrastructural level of a GFP-Myo6-CBD–positive melanosome identified by CLEM.** 3D model obtained from manually drawn contours of tomogram showed a tubular structure in continuity with the limiting membrane of the melanosome (red). This melanosome was identified by CLEM as positive for GFP-Myo6-CBD (see also Fig. 3 C). Note that the melanin-positive fibrils (black) did not enter within its lumen. Video is shown at seven frames per second.

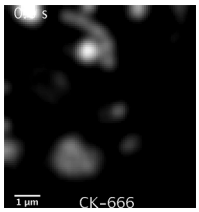

Video 7. **Inhibiting Arp2/3 activity prevents the release of VAMP7 tubules from melanosomes.** Spinning-disc confocal microscopy on MNT-1 cells expressing mCh-VAMP7 and incubated for 30 min with 50 µM CK-666 shows two melanosomes (arrows) associated each with a VAMP7⁺ tubular structure (arrowheads) unable to detach over time acquisition (see also Fig. 4 I). Acquisition parameters: 200 ms exposure, one z-stack (0.2 µm). Video is shown at seven frames per second. Bar, 1 µm.

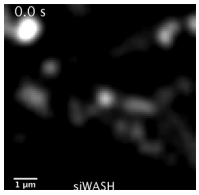

Video 8. **WASH depletion impairs the release of VAMP7 tubule from melanosome.** Spinning-disc confocal microscopy on WASH-depleted MNT-1 cells expressing mCh-VAMP7 shows a VAMP7⁺ tubular structure (arrowhead) associated with the melanosome (arrow). The tubule stays associated with the melanosome core and fails to detach over time-acquisition (see also Fig. 5 A). Acquisition parameters: 200 ms exposure, one z-stack (0.2 µm). Video is shown at seven frames per second. Bar, 1 µm.

References

Anderson, R.G.W., J.R. Falck, J.L. Goldstein, and M.S. Brown. 1984. Visualization of acidic organelles in intact cells by electron microscopy. *Proc. Natl. Acad. Sci. USA.* 81:4838–4842. https://doi.org/10.1073/pnas.81.15.4838

Raposo, G., D. Tenza, D.M. Murphy, J.F. Berson, and M.S. Marks. 2001. Distinct protein sorting and localization to premelanosomes, melanosomes, and lysosomes in pigmented melanocytic cells. *J. Cell Biol.* 152:809–824. https://doi.org/10.1083/jcb.152.4.809